Table of contents:

Captions for:

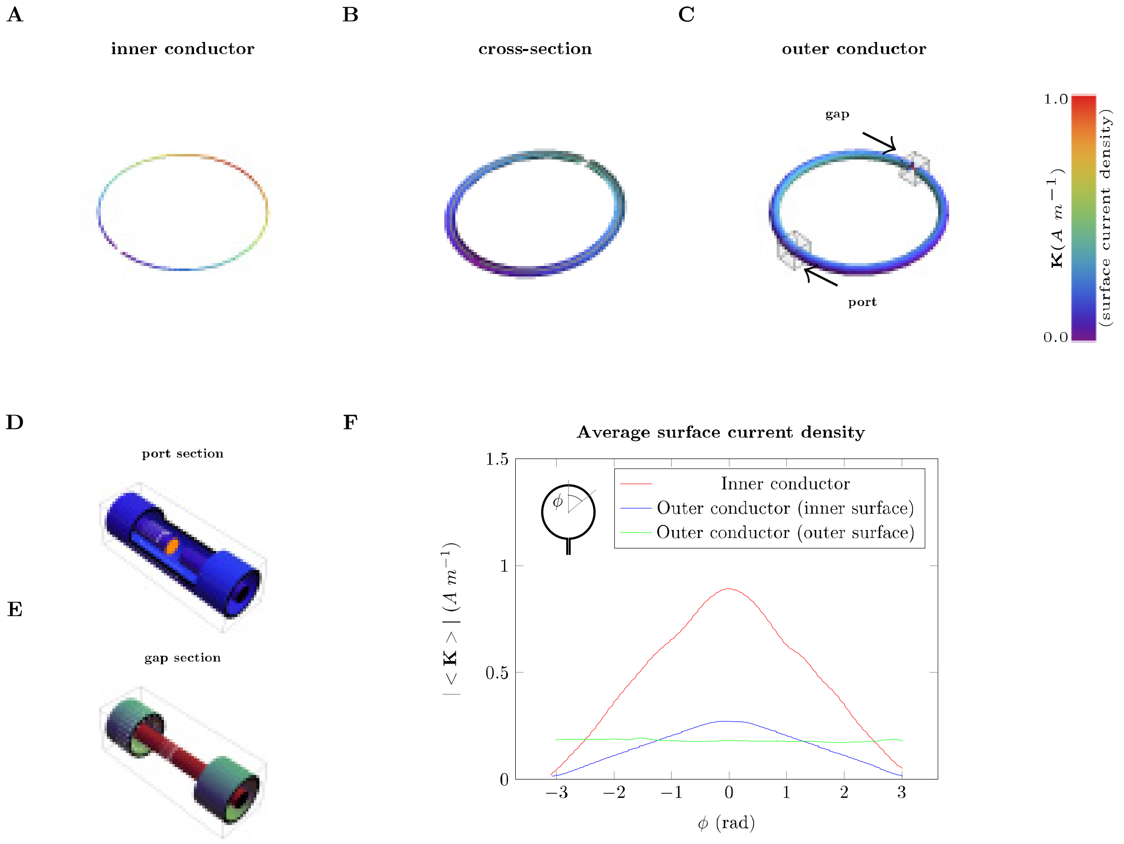

Supplemental Figure 1: The surface current density (K) distribution on a simplified 8cm diameter HIC coil. Simulations were performed using CST microwave studio (Darmstadt, Germany), assuming radiative boundary conditions and perfect conductors. A: The surface current density on the conductor. B: The cross-section revealing the surface current distribution on the inner surface of the outer conductor. C: The surface current distribution on the outer surface of the outer conductor. D: Illustrations showing the gap in the inner conductor at the port. In the simulation the outer conductor completely encases the inner conductor, for displaying purposes only half the outer conductor is shown. E: Illustrations showing the flow of current around the gap in the outer conductor. White arrows indicate the direction of the current flow. F: Plot of the average surface current distribution as a function of ϕ.

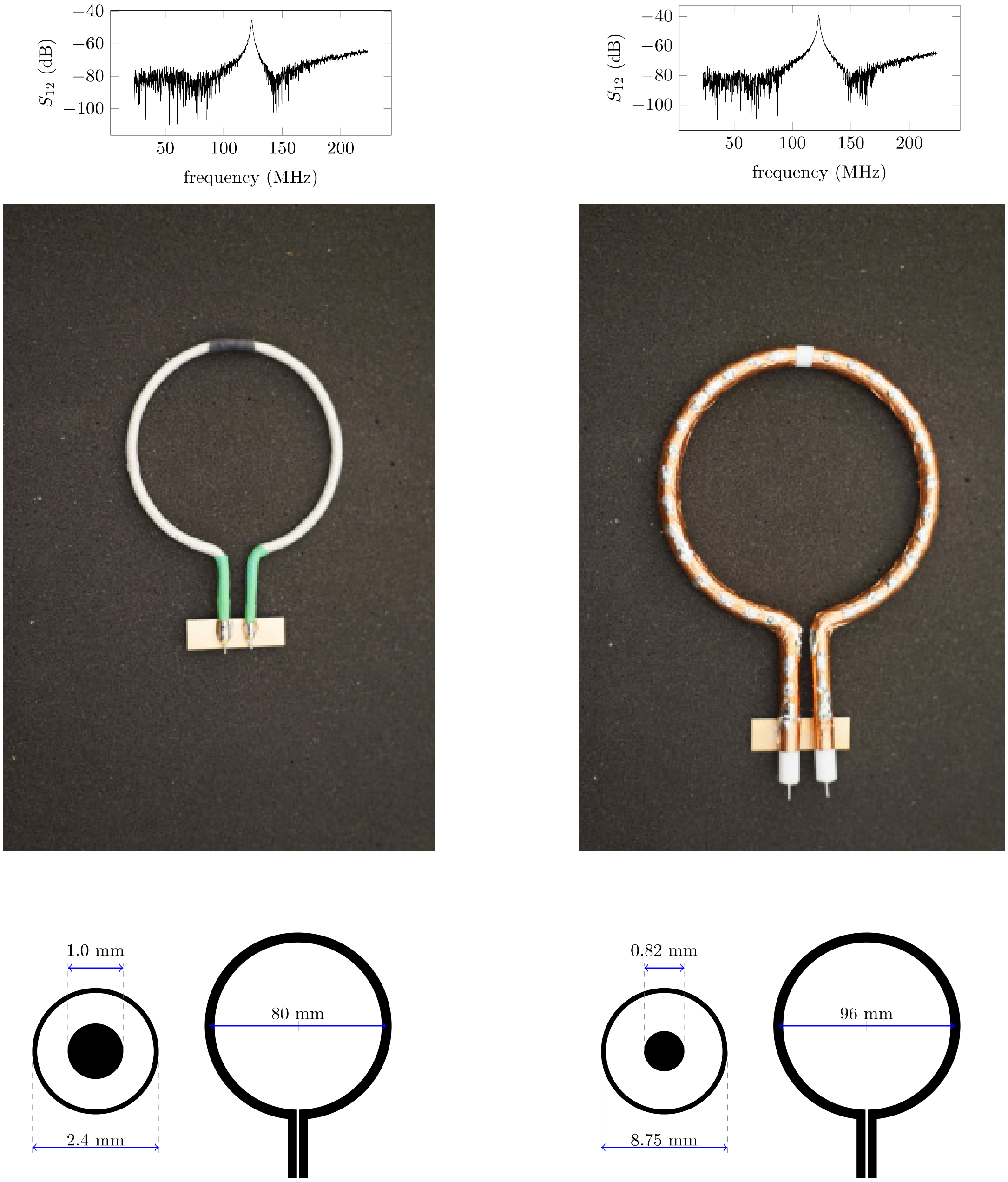

Supplemental Figure 2: Comparison of two 3D printed HIC elements resonating at the same frequency. The ratio between the inner and outer diameter influences the length needed to achieve the resonance frequency. The top row shows the $S_{1,2}$ trace measured on the bench using a double-probe.

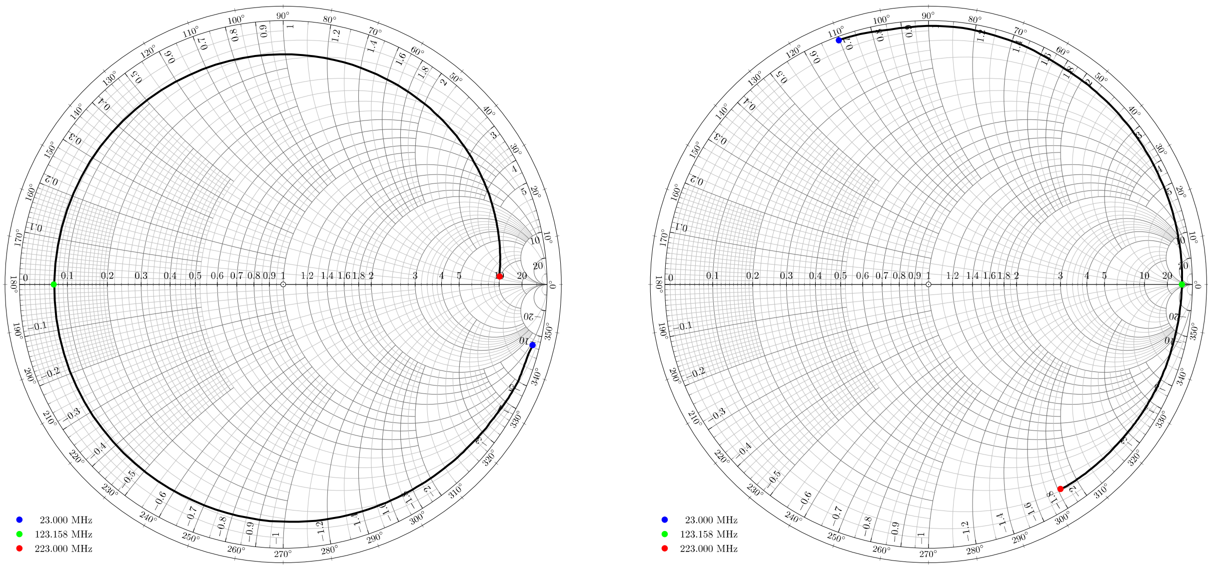

Supplemental Figure 3: Smith charts for the low impedance coil (left) and the high impedance coil (right). The green marker indicates the proton resonance frequency corresponding to the proton frequency in our 3 Tesla MRI system. The low and high impedance coils have a characteristic impedance of 11Ω and 2429Ω, respectively. Measurements were performed while the coil was placed on top of a large cuboid phantom (317x317x104mm). The conductivity of the liquid inside the phantom was 0.53 S/m.

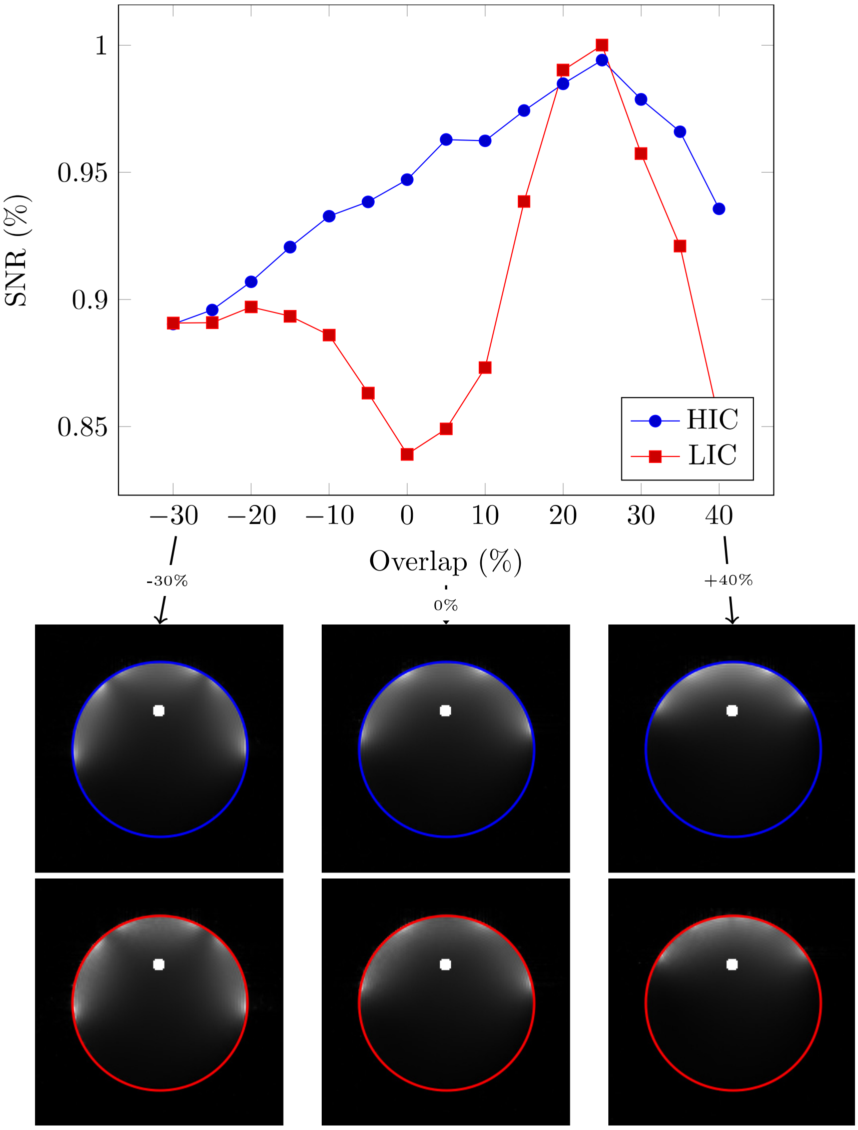

Supplemental Figure 4: Evaluation of SNR degradation due to coupling between neighboring coil elements as a function of coil overlap on a cylindrical surface (16.9cm diameter). The blue (HIC measurements) and red (LIC measurements) lines shows the SNR at 4.2cm below the center coil in a three-coil arrangement. The overlap between coils is varied between -30 and +40%, where the % overlap is computed from the element diameter. The MR images below the graph show the combined signal images at -30, 0 and +40% overlap. The blue (HIC data) and red (LIC data) outlines superimposed on the MR images mark the edges of the phantom. The white dot indicates the position of the SNR measurement. The reduced SNR degradation for the LICs on the cylindrical surface may be explained by the increased orthogonality of the coil elements as the angle increases (at -30% overlap, the coils are almost at a 90° angle to one another).

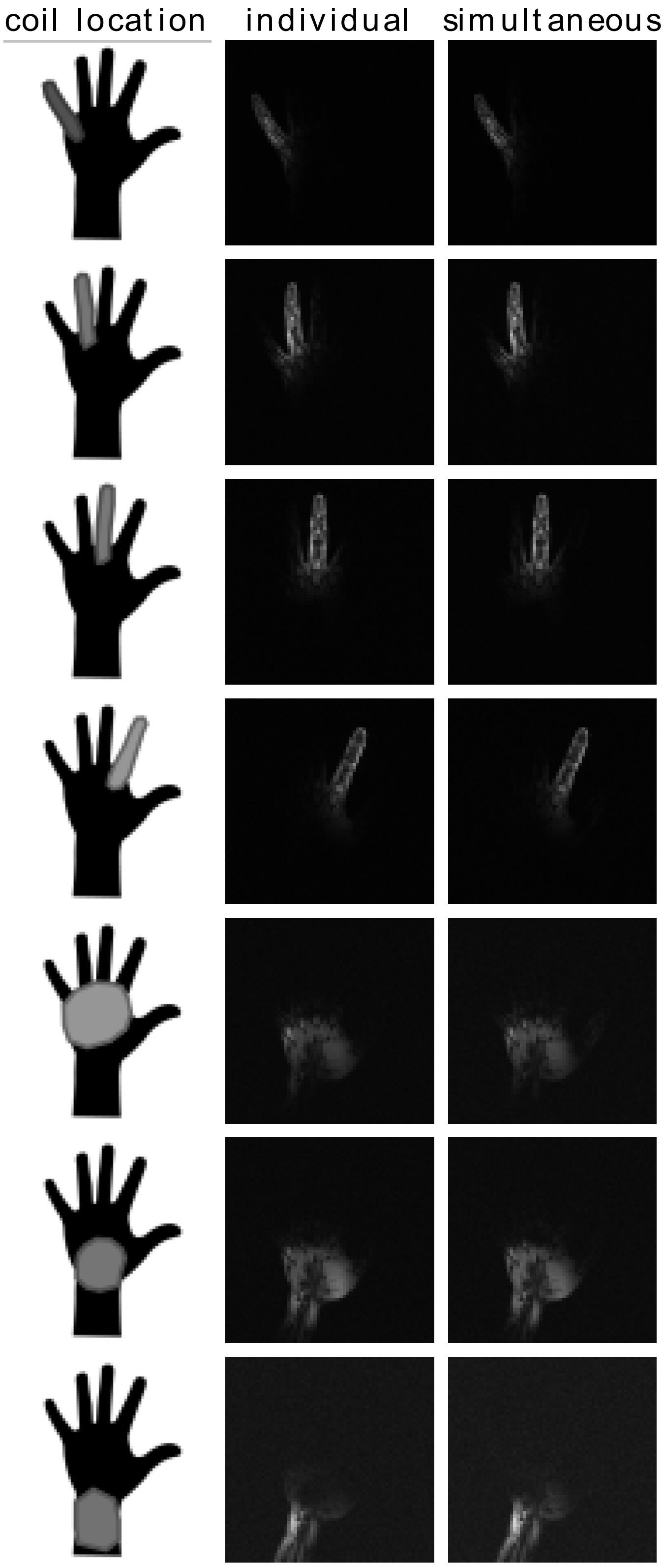

Supplemental Figure 5: Evaluation of signal coupling between HIC elements in the glove coil. Gradient recalled echo images acquired in 8 separate measurements, each with only one coil activated at a time (center column). Gradient recalled echo images acquired in one single measurement with all coils activated at the same time (right column). Each row is displayed at the same scale. Sequence parameters: TR=10ms, TE=3.72ms. flip angle = 25, 512x512 Matrix, 265x265mm FOV, 2mm slice thickness, 0.5x0.5mm resolution, total scan time = 5 s.

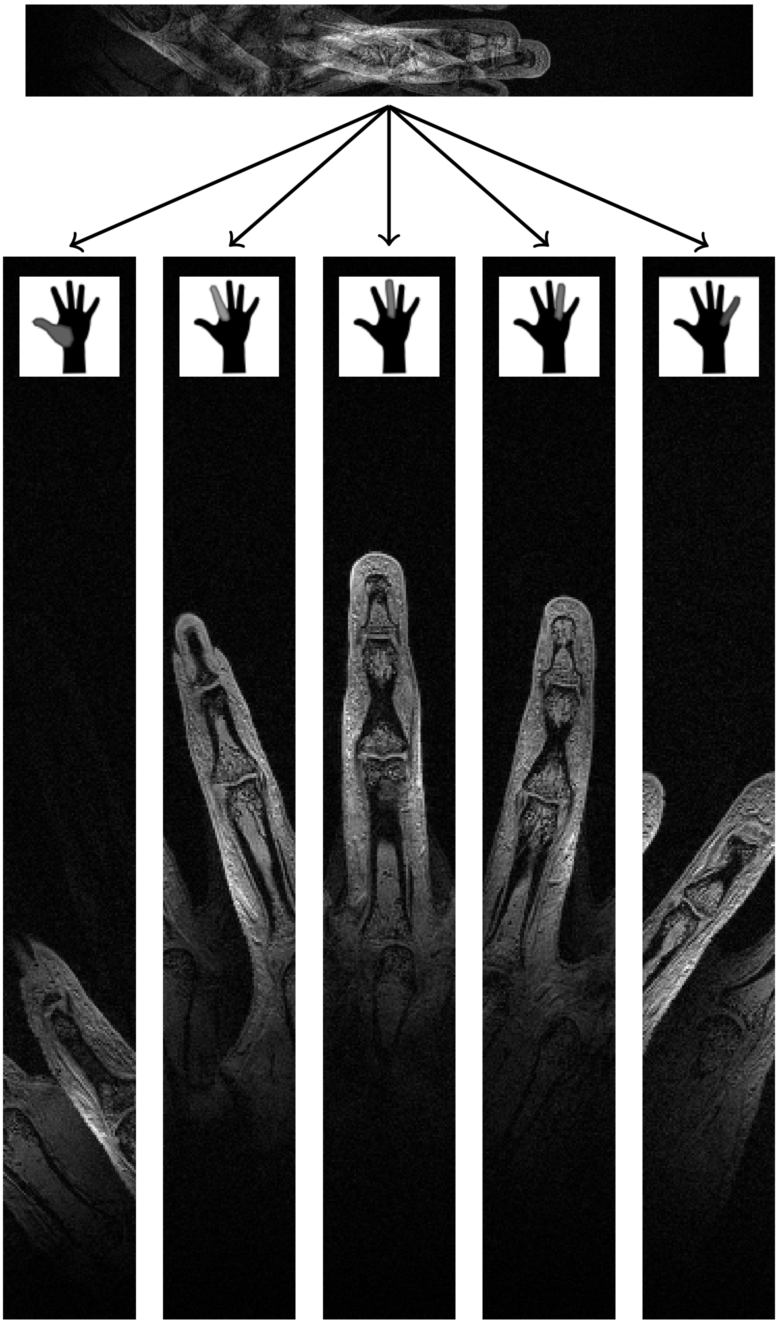

Supplemental Figure 6: A 3D data set (non-selective excitation) acquired covering only the middle finger. The top panel shows a central slice from the 3D data set combining all data from all coils. Underneath the top panel, each of the individual coil images (measured simultaneously) are placed side by side to reveal the individual fingers. Note that, no parallel imaging reconstruction techniques were used to separate the images. (0.5 mm isotropic, 512x64x104 matrix, 256x32x52 mm field of view, TR = 12ms, TE = 5ms, 10 degree flip angle, total scan time 1min 20sec).

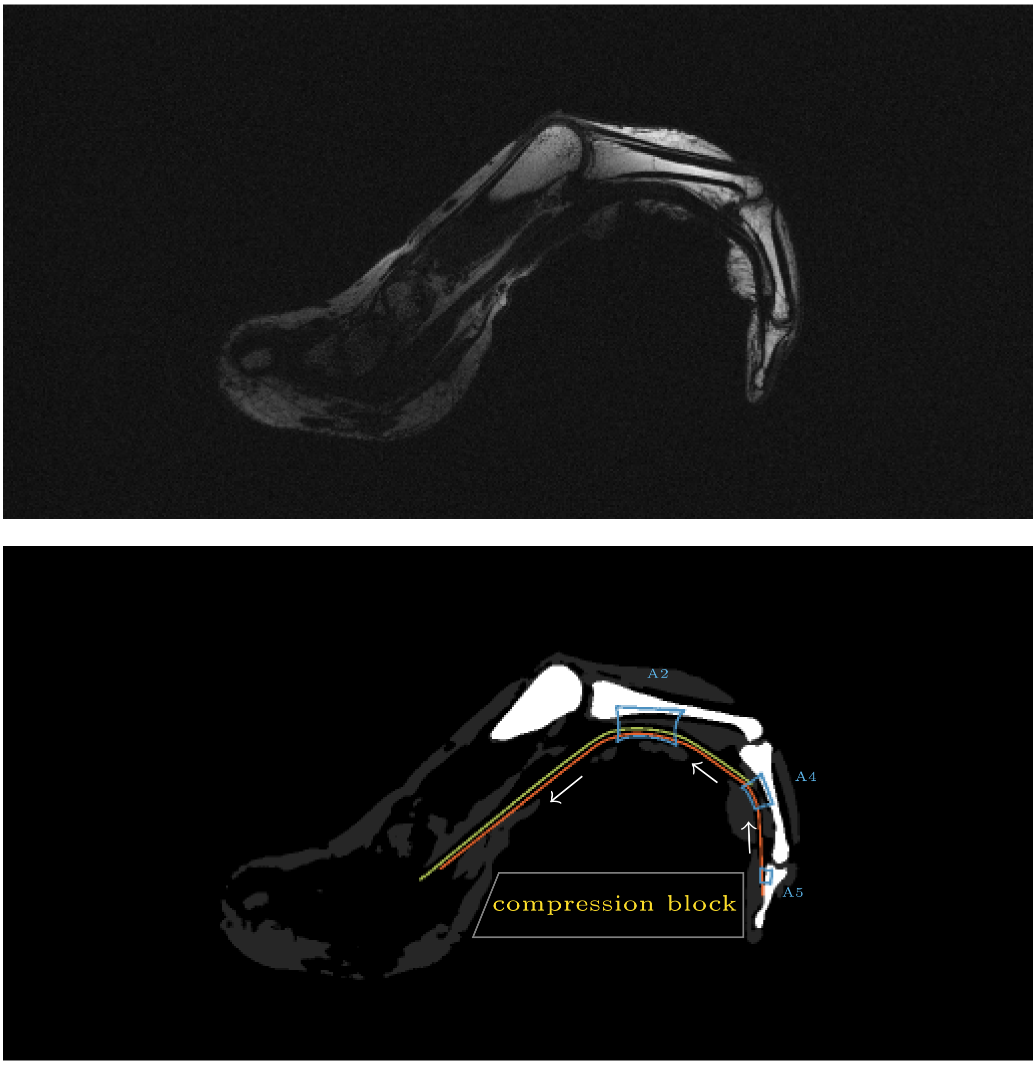

Supplemental Figure 7: Sagittal T1 weighted image through the flexor tendon in the index finger while squeezing a block of wood (top penal). Although pulley ligaments and flexor tendon are almost indistinguishable based on underlying contrast (both have short T2 relaxation times), their interaction can now be revealed. As the subject squeezes on the compression block, the load on the flexor tendon is distributed over the pulleys as illustrated in the bottom panel.

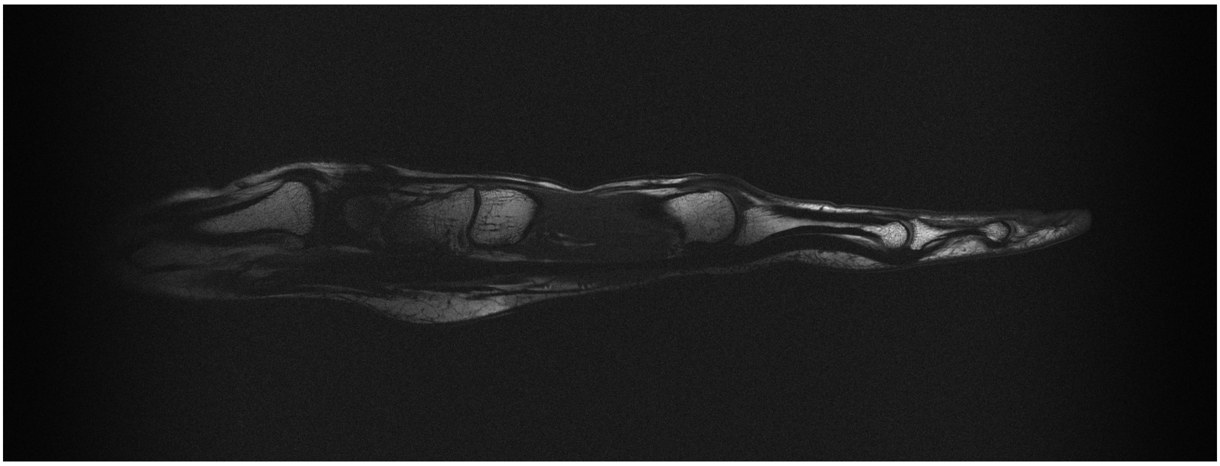

Supplemental Figure 8: Sagittal T1 weighted image through the flexor tendon in the index finger while the hand is stretched out. Sequence parameters: TR=400ms, TE=15ms, excitation angle = 90, refocusing angle = 180, Turbo factor 2, 2024x512 Matrix, 303.6x76.8mm FOV, 2mm slice thickness, 150x150 µm resolution, total scan time = 1min 42s.

Supplemental Figure 9: Sagittal T1 weighted image through the flexor tendon in the index finger while the hand is holding a peach. Sequence parameters: TR = 400ms, TE = 15ms, excitation angle = 90, refocusing angle = 180, Turbo factor 2, 2024x512 Matrix, 303.6x76.8mm FOV, 2mm slice thickness, 150x150 µm resolution, total scan time = 1min 42s.

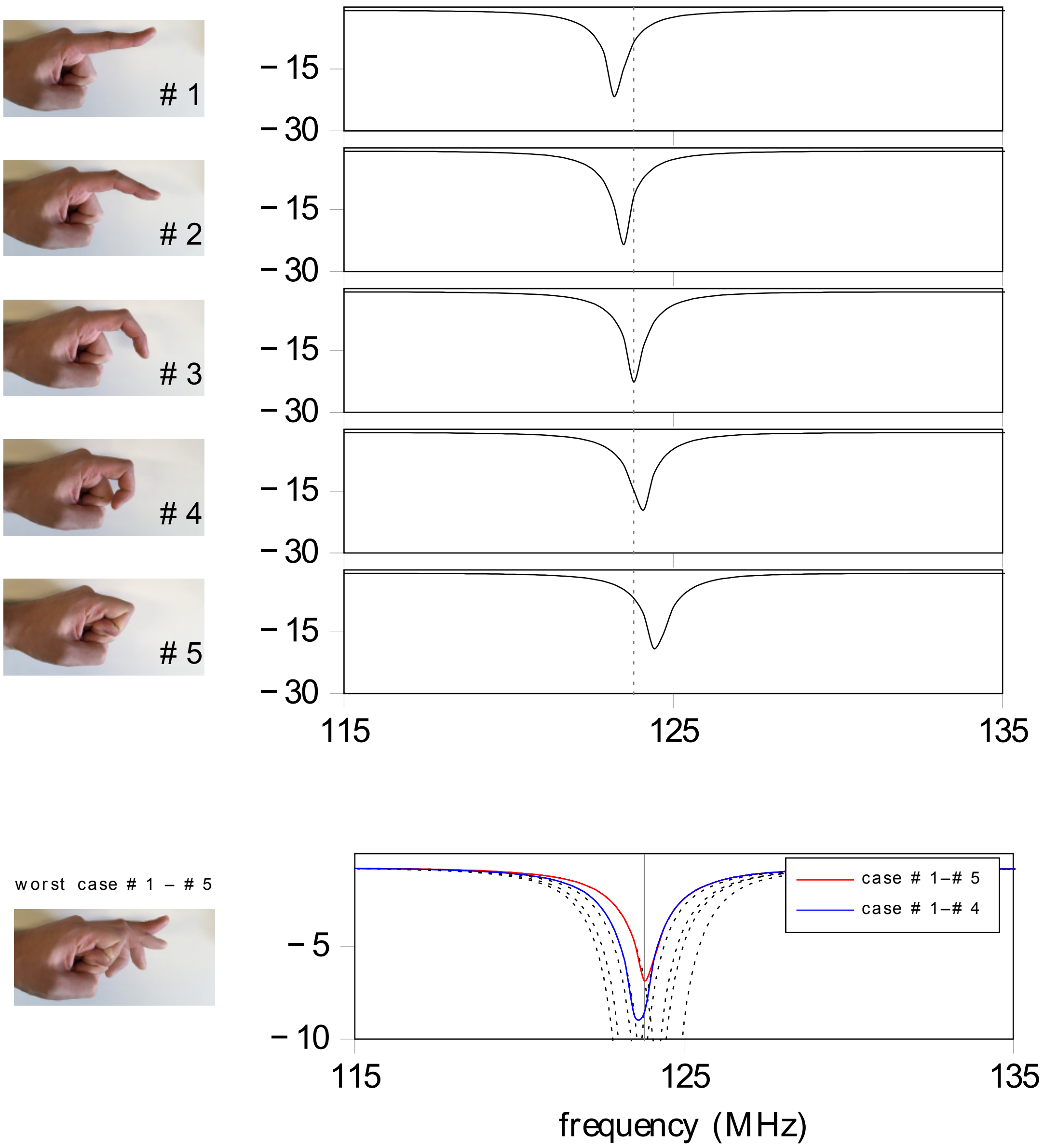

Supplemental Figure 10: The $S_{1,1}$ of one of the finger elements in the glove coil measured on the bench with the finger in different positions (top 5 rows). Note that the coil was tuned to the slightly bent position (#3). The bottom row shows the worst case among all positions (red) and the first conditions #1-#4. Only when the finger is completely bent in on itself (#5) does the $S_{1,1}$ drop below -9dB at the frequency of interest.

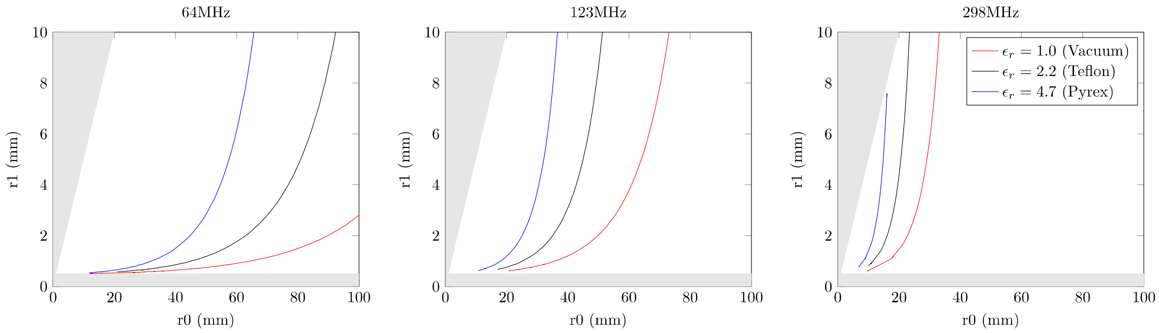

Supplemental Figure 11: Possible dimensions (coil radius r_0 and substrate radius r_1) for HIC designs using different substrate materials (vacuum ε_r = 1.0, Teflon/Polyethylene ε_r = 2.2, Pyrex ε_r = 4.7). From left to right, solutions for 64MHz (1.5 Tesla), 123MHz (3 Tesla), and 298MHz (7 Tesla), respectively, are shown. The x-axis shows the radius of the loop (r_0 in Eq. 3). The y-axis shows the radius if the substrate (r_1 in Eq. 3). In these calculations, the thickness of the inner conductor was set to 1mm. Consequently, r_1 must be larger than 0.5 mm. Similarly, r_1 must also be smaller than 0.5 × r_0. These non-physical areas ($r_1 \leq 0.5$ & $r_0 \leq 2 \times r_1$) are marked in gray.

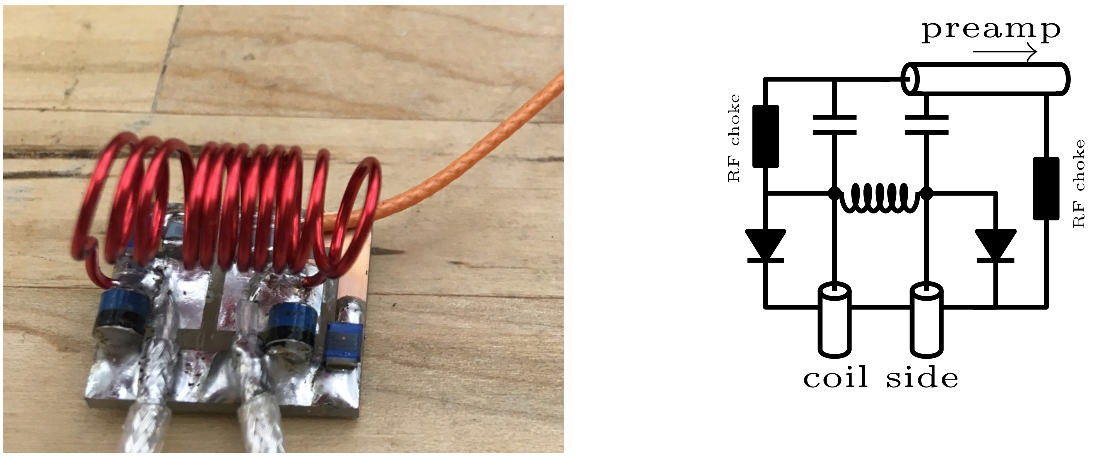

Supplemental Figure 12: Photo of the HIC interface board (left) and corresponding schematic layout (right).

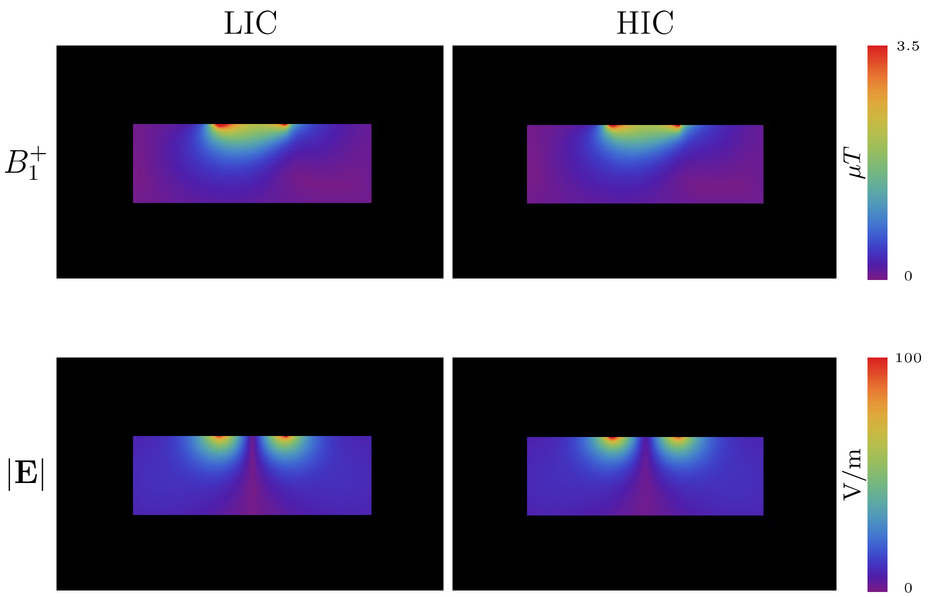

Supplemental Figure 13: Simulated ||**E**|| and B_1^+ fields in a large cuboid phantom (coronal slice through the center of the coil). The current distribution on the outside of the HIC (when the reversed pre-amplifier decoupling is deactivated) is almost identical to the traditional loop. Hence, both coils produce almost identical **B** and **E** fields. This observation is in agreement with the nearly identical single coil baseline SNR measured in our single LIC and HIC coil experiments (supplemental figure 15) and similar individual coil images in figure 2 of the main paper.

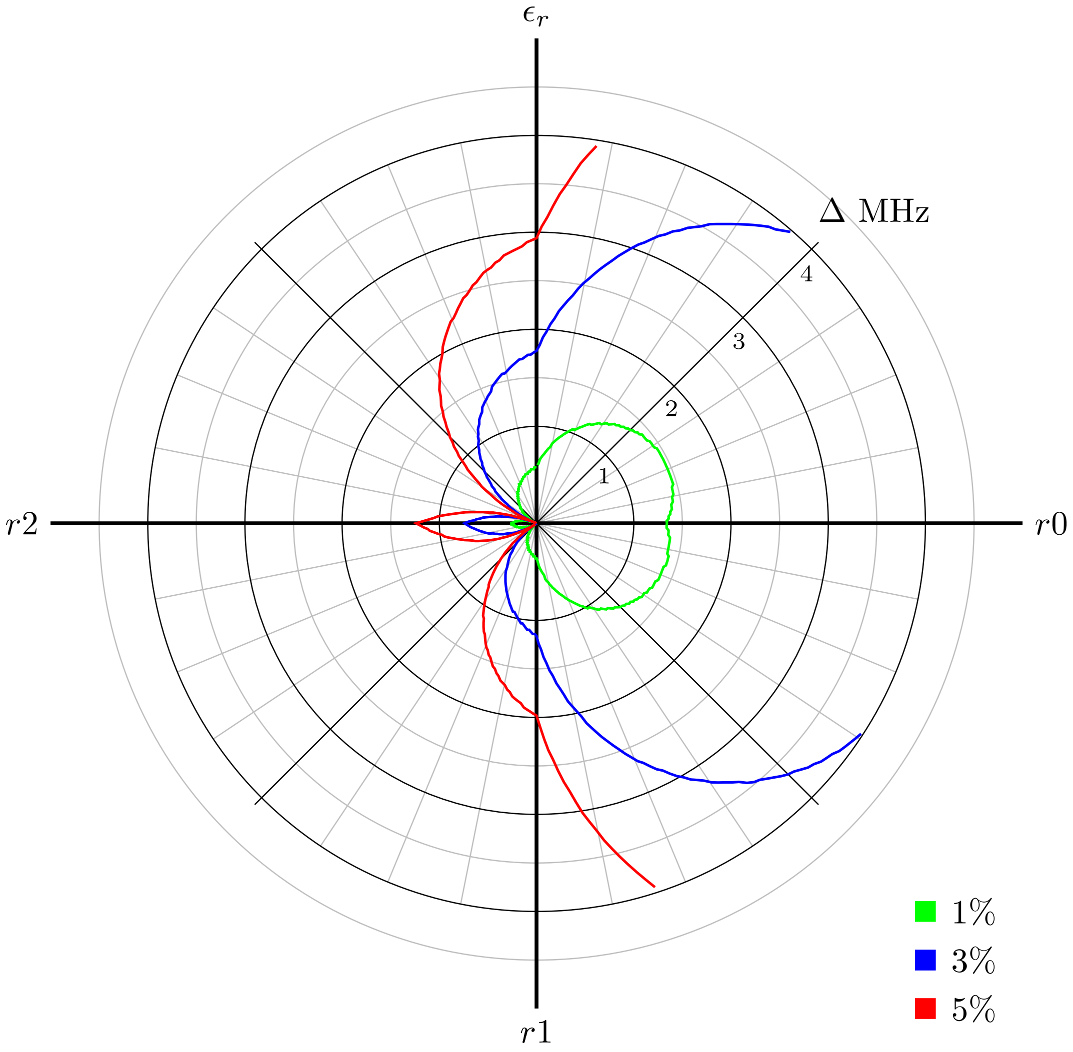

Supplemental Figure 14: Deviation from the target frequency as a function of variation in material properties/dimensions for an 80mm diameter 123MHz HIC using $\varepsilon_r = 2.2$ (the same value as for the 3D printed HIC elements in the paper). The green, blue and red lines indicates a 1,3, and 5% change from the design, respectively. Deviations in r_1, r_2 and ε_r have a reliably small effect compared to deviations in r_0. It should be noted, however, that a 1% change in r_0 translates to a 2.5mm change in coaxial length, which can easily be adjusted by trimming the coaxial stubs to the correct length on the bench.

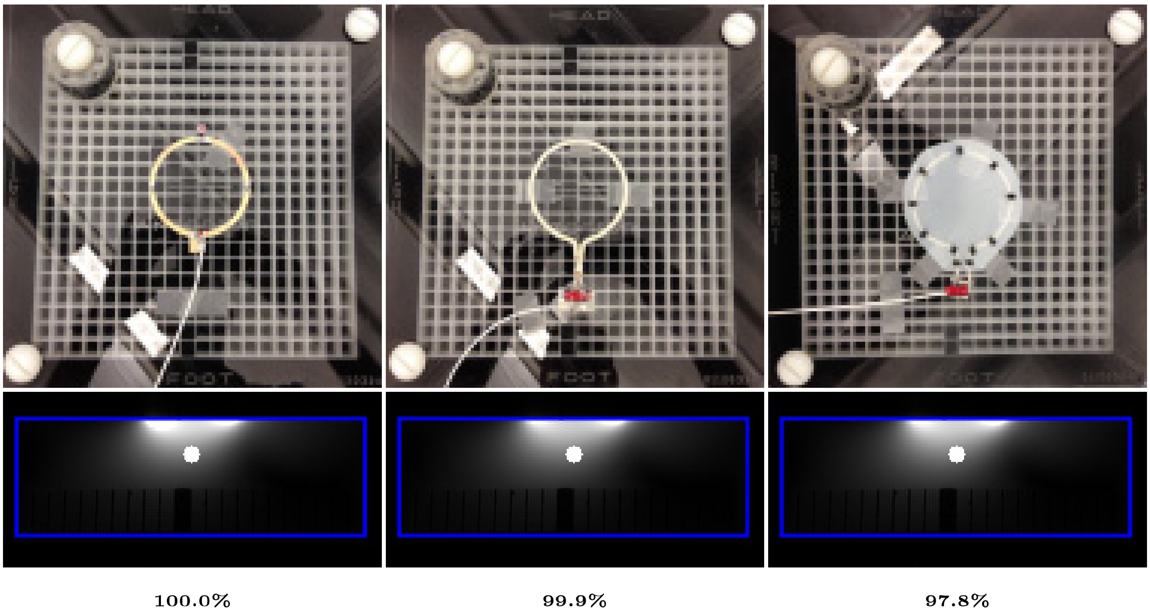

Supplemental Figure 15: Evaluation of the signal to noise ratio relative to a traditional 8cm low impedance coil element. From left to right: 8 cm low impedance coil, 8cm 3D printed high impedance coil, and a high impedance coil fabricated from RG178. The number underneath each column indicates the relative SNR measured at 42mm depth compared to the 8cm traditional low impedance coil.

Captions of supplemental videos:

Supplemental Video 1: MR video showing a coronal slice through the left hand while the subject moves her fingers in a motion pattern similar to playing the piano or typing on a keyboard (0.8x0.8mm in-plane resolution, 2.5mm slice thickness).

Supplemental Video 2: MR video of the left hand grabbing an object (peach). The imaging plane is centered on the peach, but there are no MR coils on the peach itself. As the hand wearing the glove coil moves through the imaging plane different parts of the hand become visible. As the hand grabs the object the coils on the glove also wrap the peach, revealing the inner structure of the fruit (0.8x0.8mm in-plane resolution, 2.5mm slice thickness).